Cryocooler based test setup for high current applications

Jedidiah Pradhan, Nisith Kr. Das, Anindya Roy, and Anjan Duttagupta

Citation: Review of Scientific Instruments **89**, 045110 (2018); doi: 10.1063/1.5020006
View online: https://doi.org/10.1063/1.5020006
View Table of Contents: http://aip.scitation.org/toc/rsi/89/4
Published by the American Institute of Physics

Cryocooler based test setup for high current applications

Jedidiah Pradhan,[a] Nisith Kr. Das, Anindya Roy, and Anjan Duttagupta
Variable Energy Cyclotron Centre (VECC), 1/AF, Bidhan Nagar, Kolkata 700064, India

(Received 19 December 2017; accepted 23 March 2018; published online 16 April 2018)

A cryo-cooler based cryogenic test setup has been designed, fabricated, and tested. The setup incorporates two numbers of cryo-coolers, one for sample cooling and the other one for cooling the large magnet coil. The performance and versatility of the setup has been tested using large samples of high-temperature superconductor magnet coil as well as short samples with high current. Several un-calibrated temperature sensors have been calibrated using this system. This paper presents the details of the system along with results of different performance tests. *Published by AIP Publishing.*
https://doi.org/10.1063/1.5020006

I. INTRODUCTION

The advent of powerful cryo-coolers[1] makes it possible to carry out low temperature measurement in different temperatures and magnetic fields without using liquid cryogens. This paves the way for a simpler cryostat and eliminates refilling of coolants. It is primarily a cryogen-free cryogenic test setup; however, provision is made to use liquid helium as well under exigent situations. The system happens to be flexible and versatile that can cater diverse requirement of different users in terms of their kinds of applications. An isothermal calorimeter provided for experimentation with small samples coupled with large magnet outside the calorimeter makes the system more useful to the users. The system is capable of measurement at variable temperatures even with high current under different magnetic fields and allows testing of widely varying dimensions, from a few millimetres to several centimetres, and effectively determines various important parameters. For instance, the optimal magnet current and operation temperature of the HTS magnet coil can be determined using this setup. With this mission in view, we have developed a conduction-cooled HTS magnet[2,3] and tested in the setup. The magnet is designed and fabricated for high current measurement at low temperature using a conduction-cooled cryogenic test bed. The Ic measurement of short HTS samples is carried out in this cryogen-free system. A similar cryogen-free system can be found elsewhere.[4]

To make it a stable and reliable system, two cryo-coolers (CC1 and CC2) have been used, one for the sample and another one for magnet cooling, respectively. Besides the basic design of the cryostat, several other factors relevant to low temperature such as thermal links, radiation heat shielding, and current leads have been optimized for maximum use of cold out of the cryo-coolers. The system consists of two thermally isolated cryo-coolers, a removable sample insert, a liquid helium chamber (~5 L), two pairs of HTS-based current leads, and a cold plate for attaching the magnet coil. Special provision has been made for easy mounting and replacing the sample without causing any cold loss. We have also designed and fabricated a laboratory-scale conduction cooled HTS magnet consisting of sixteen numbers of pancake coils, each inserted between copper plates. Successful testing of the magnet and HTS-based current leads in the system validates its performance. We have characterised the HTS tape at various temperatures for critical current.[5] This system is used for calibration of several temperature sensors, measurement of Residual Resistivity Ratio (RRR) for niobium samples, and characterization of small magnetic samples.

II. EXPERIMENTAL SETUP AND PROCEDURES/ MATERIALS AND METHODS

A. Housing cryostat

The test setup allows us to measure electrical characteristics of assorted samples under large transport current. The basic functions include cooling the sample to temperature as low as 4 K, transporting current in the range of 0-400 A under different magnetic fields. The cryostat for the setup is composed of two close cycle cryo-coolers, a removable sample-mount, HTS-based current leads, a superconducting magnet, and a temperature controller. It is about 1.2 m long and 600 mm diameter and is placed on a movable table as shown in Fig. 1. A central port of diameter 250 mm at the top plate is used for sample mounting using a centre stick of about 12 kg weight and can be removed/installed manually as shown in Fig. 1. Circular copper plates of larger diameter, rigidly fixed to the cold heads of the cryo-cooler, act as thermal capacitors for distribution of cold loads to different sub-systems. A sample space (70 mm $\varphi \times 250$ mm) is surrounded by an iso-thermal copper shield (calorimeter) for maintaining uniform temperature and it can also be filled with liquid helium, if necessary. A sample mount inside the sample space is constructed that would help conduct heat away from the sample and ensuring proper thermal contacts. The sample is electrically insulated from the sample mount with the Kapton tape and coated with thermal compound to improve thermal conductivity. The large sample space offers a longer sample length for measurement to improve the signal-to-noise ratio under test. Two numbers of Gifford MacMahon (GM) cryo-coolers, CC1 and CC2, with water cooled compressor systems are dedicated for cooling the

[a]jpradhan@vecc.gov.in

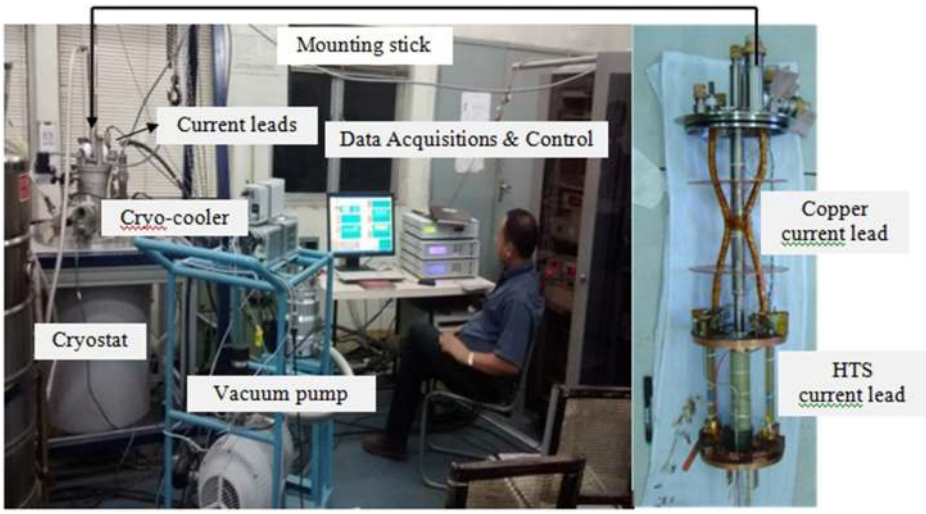

FIG. 1. Test setup and the sample mounting stick.

sample mount and magnet coil, respectively. The cryo-coolers act as a heat sink to cool-down the cold mass to operating temperature. The 1st stage of the cooler, CC2 attached to the magnet, provides cooling to the aluminium thermal shield and intercepts heat loads from structural supports and electrical wiring. For measurement of temperature, several temperature sensors are installed on the sample mount, cold heads, and along the thermal path to measure the temperature inside the cryostat. The sample temperature is controlled by a temperature controller (Lakeshore model 338) connected to the temperature sensor placed on the sample mount. A pair of binary current lead, which is a series combination of a normal conductor (copper) from room temperature to first stage temperature followed by the HTS conductor from first stage temperature to second stage temperature, carries current to the magnet and sample, respectively.

We solve the energy balance equations so as to optimize the distribution of thermal loads out of two cryo-coolers (CC1 and CC2) keeping the second stage isolated. In the present context, we consider four major components, viz., a radiation shield, first thermal anchor, superconducting magnet, and second thermal anchor. The thermal anchor is the extended copper plate attached to the cryo-cooler cold head. The internal structure and cryogenic load distributions of both thermally isolated magnet and sample circuit are shown in Fig. 2, respectively. An analytical model consisting of heat conduction equations including a Joule heating term for each thermal component is given by[6]

$$\frac{d(CT)_s}{dt} = Q_H - Q_{A1} - Q_L, \tag{1}$$

$$\frac{d(CT)_{A1}}{dt} = Q_{A1} - Q_{C1}, \tag{2}$$

$$\frac{d(CT)_M}{dt} = Q_L - Q_{A2}, \tag{3}$$

$$\frac{d(CT)_{A2}}{dt} = Q_{A2} - Q_{C2}. \tag{4}$$

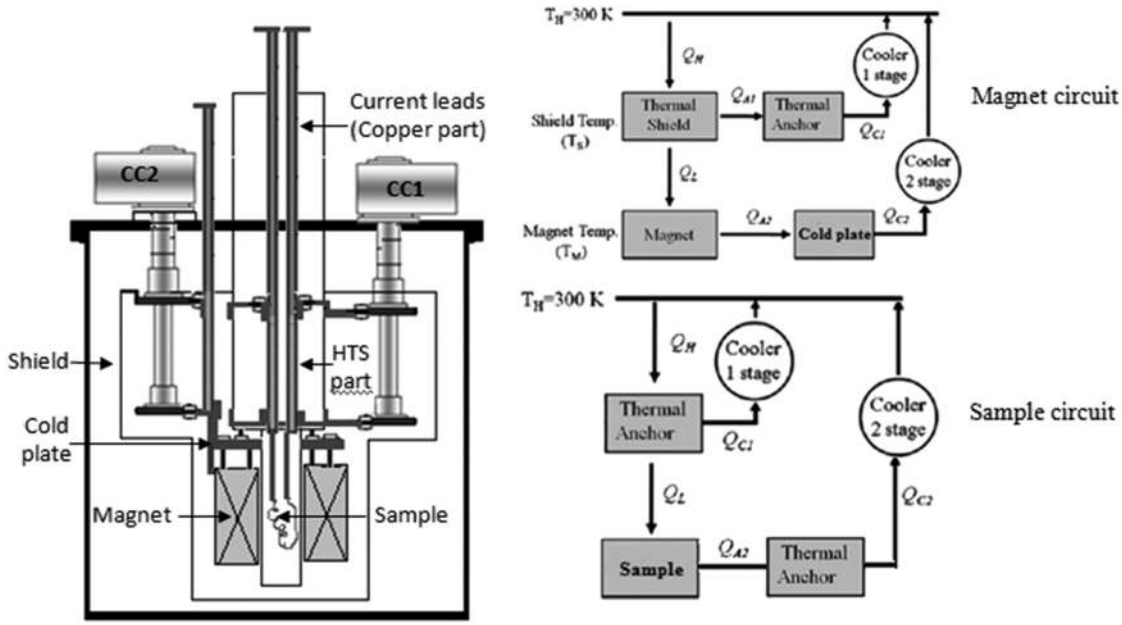

FIG. 2. Schematics of the test setup showing heat flow under a two-stage cryo-cooler consisting of two isolated thermal circuits.

TABLE I. Calculated heat loads of two cryocoolers (CC1 & CC2).

First stage of cryo-cooler	Heat load-CC1	Heat load-CC2
Copper leads	40 W at 500 A	24 W at 300 A
Support/penetrations (W)	1	2
Radiation (W)	4	5
Second-stage of cryo-cooler		
HTS current leads (mW)	250	150
Support/penetrations (mW)	180	70
Radiation (mW)	50	50

The meaning of the symbols used in the calculation is given in the Nomenclature.

In most cryogenic applications, effective heat transfer occurs through thermal conduction along mechanical support, thermal radiation, and conduction due to the residual gas. In addition, Joule heating in electrical leads, eddy current heating, mechanical vibration, adsorption, or desorption of gases may significantly contribute to the heat transfer. In the energy balance equation, Q_H and Q_L denote the cryogenic load from room-temperature, T_H, to first-thermal shield temperature, T_S, and magnet temperature T_M, respectively. Major heat transfer processes are support conduction, Q_k, thermal radiation, Qr, heat through current lead, Q_l, and gas conduction, Qg (negligible under a good vacuum)

$$Q_H = Q_{k1} + Q_{r1} + Q_{l1}, \tag{5}$$

$$Q_L = Q_{k2} + Q_{r2} + Q_{l2}. \tag{6}$$

The contribution of heat loads from different sources at two temperatures corresponding to 1st and 2nd stages of the cryo-cooler is shown in Table I.

When a two-stage cryo-cooler is used, coupling of two stages of the cryo-cooler makes the estimation of actual cooling capacity rather complicated.[7] The empirical cooling capacity of a two-stage GM cryo-cooler is used for this numerical analysis. The simulation uses the temperature-dependent thermal conductivity and specific heat of each component in the system and refrigeration capacity as the input during cool-down. The initial cool-down characteristics are affected by the dimension of thermal links because the amount of heat flow increases with heat transfer area. However, the cooling efficiency of thermal links decreases because the increased cross-sectional area resulting in heavier weight requires more cooling capacity. The cross section for a given length of thermal links is optimized considering the cooling capability of the cryo-cooler.

The reduction of temperature during cooling down is carried out using the TAK-2000 (Thermally Analysis Kit) code based on finite difference method.[8] The analysis is carried out under both steady and transient conditions.

B. The current lead

A modular design of current lead consisting of high temperature superconductors (HTSs) to reduce resistive losses is introduced between the two stages of the cryo-cooler. Two binary pairs of current leads are used in the system, one for the sample and the other one for the magnet coil. Thermal anchors with electrical isolation are provided between the cryo-coolers and the current leads in order to provide the thermal connection to the sample. A design of current lead is critical owing to large Joule heating under a limited cooling power. The sample current lead is capable to carry 400 A of current in a sample under test while keeping the sample cold. Another pair of current lead supplies current to the magnet. These HTS leads terminate at the copper blocks of the sample mounting system, however electrically isolated from the cold head by anodized aluminium as shown in Fig. 3. The copper current lead between the first stage and room temperature happens to be the major contributor of heat to the system. The size of the copper current lead between the room temperature flange and the first stage of the cryo-cooler was optimized for minimum conduction heat load and joule heat generation. The current limitation to the sample is determined by the cooling capacity of the 1st stage due to the large resistive heating of the upper copper leads under vacuum. Thermal anchors with large

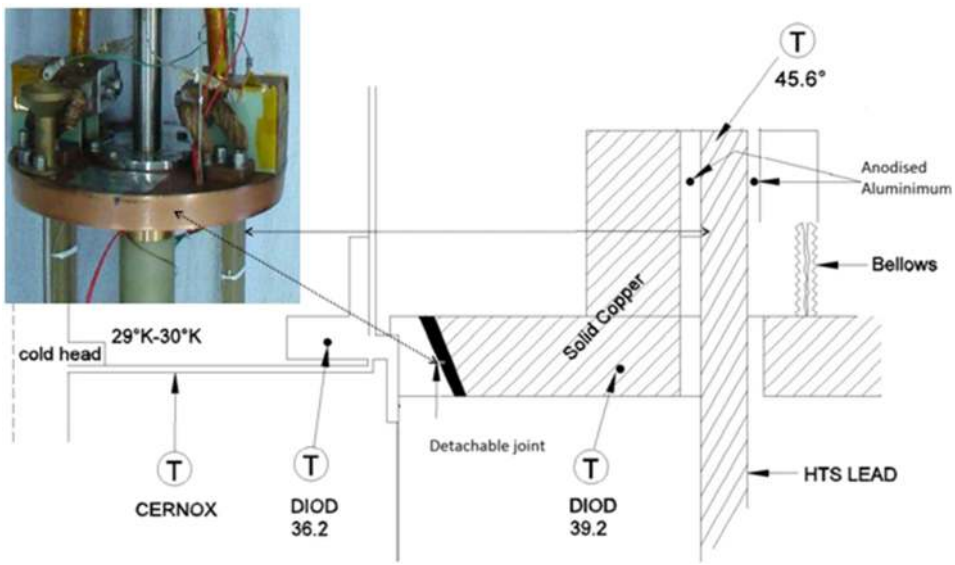

FIG. 3. The current lead junction and temperature as measured at different locations.

contact surface area are used to thermally connect the current leads at the 1st and 2nd stages in conjunction with flexible thermal links. This is to ensure efficient heat transfer to the first stage with higher current and to reduce the heat load to the second stage. The details of the detachable joint along with measured temperatures at different locations are shown in Fig. 3.

For optimisation of the current leads, we consider a one-dimensional model for power dissipation within a current lead carrying a transport current I,

$$\frac{d}{dz}\left[Ak(T)\frac{dT}{dz}\right]+\frac{\rho(T)[I-I_c(B,T)]^2}{A}=C(T)A\frac{dT}{dt}, \quad (7)$$

where z is the axial distance along the lead, z = 0 at the cold end. Ic is the critical current of the HTS tape under magnetic field B and temperature T. The temperature at z = 0 is determined by the cooling power of the 2nd stage of the cryo-cooler while the other end is fixed at 300 K. The junction between the HTS and copper part is cooled by the 1st stage of the cryo-cooler and heat transfer is assumed to be perfect. The cooling capacity of the two-stage GM cryo-cooler is expressed by combination of the first and the second stage temperature.[7] Equation (7) for the copper part of the current lead under steady state, $\frac{dT}{dt}=0$, reduces to equation

$$\frac{d}{dz}\left[Ak(T)\frac{dT}{dz}\right]+\frac{\rho(T)I^2}{A}=0. \quad (8)$$

Equations (7) and (8) are solved numerically under steady state ($\frac{dT}{dt}=0$) for different current values having fixed temperature, T = 300 K at the room temperature side of the copper lead. Figure 4 shows the temperature variation along the length of the current lead under different current loading. As the high and low temperatures are determined by the capacity of the cryo-cooler and the length of the copper leads is fixed by the available space within the cryostat, we need to optimise the cross-sectional area of the copper lead. The optimised lead for a given current (400 A) has smooth decrease of temperature at the room temperature side and the current beyond it exceeds 300 K (see Fig. 4). For a normal conductor, changing variable to $s=k(T)\frac{dT}{dz}=\frac{Q}{A}$, in Eq. (8), reduces to

$$\frac{ds}{dz}+\rho(T)J^2=0$$
$$\Rightarrow s\,ds=-k\rho J^2 dT.$$

Integrating from T_c to T_h and Q_c is minimum when $Q_h=0$,

$$Q_c^{\min.}=I\left(2\int_{T_c}^{T_H}k(T)\rho(T)dT\right)^{0.5}\Rightarrow\frac{Q_c^{\min.}}{I}$$
$$\approx 0.042(\frac{watt}{amp}),\ \text{for copper,} \quad (9)$$

since $Q_c=k(T)A\frac{dT}{dz}\,at\ T=T_c$.

So, $dz=\frac{kA\,dT}{\sqrt{2}I\left(\int_T^{T_H}k\rho dT\right)^{0.5}}$.

As T is lowered, the length required to produce $Q_c^{\min.}$ at T_c is given by

$$\frac{L}{A}=\frac{1}{I\sqrt{2}}\left[\int_{T_C}^{T_H}\frac{k(T^*)}{\left(\int_{T^*}^{T_H}k(T)\rho(T)dT\right)^{0.5}}dT^*\right]\Rightarrow\frac{LI}{A}$$
$$\approx 40\,000\,(\frac{cm\,.\,Amp}{cm^2})\ \text{for copper.} \quad (10)$$

This is the optimum dimension of the copper lead of length L for a given A. Whereas the HTS part of current leads was designed and fabricated using Bi-2223 tapes with low thermal conductivity gold alloy stabilizers to minimise the conduction load, an Fibreglass Reinforced Plastic (FRP) support base with a cover plate and two copper terminal blocks.

We have investigated the possible quenching of the HTS current lead that may arise from current overloading or cryo-cooler mal-functioning. This would lead to an increase of warm

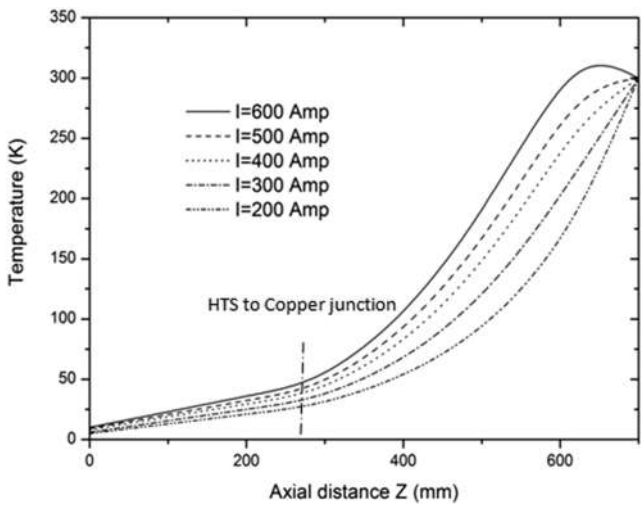

FIG. 4. Temperature profile along the current lead under five different currents.

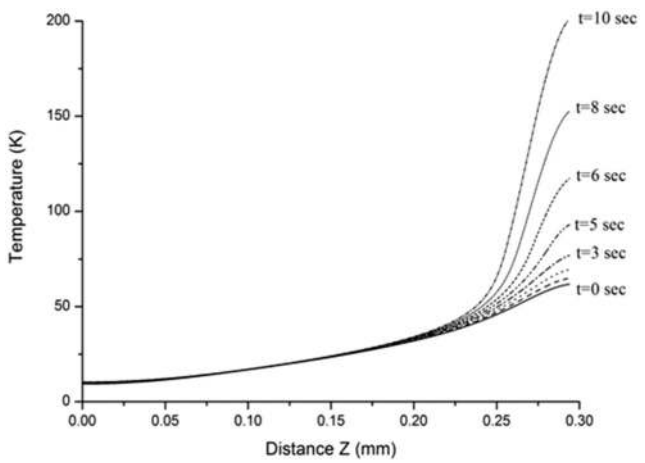

FIG. 5. Increase of temperature due to quench of the HTS part of the lead at different time intervals.

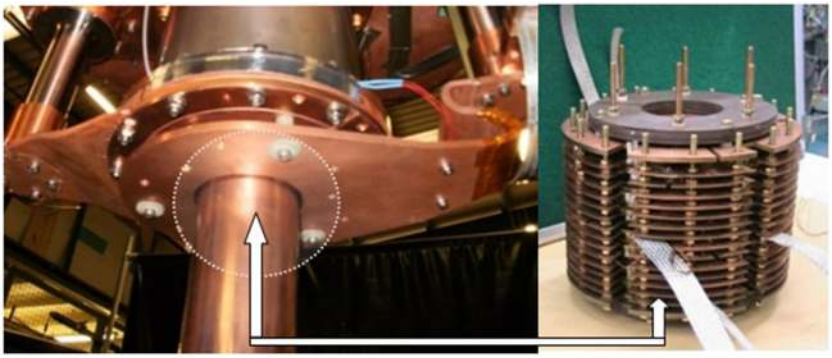

FIG. 6. Arrangement for holding and cooling the HTS magnet coil assembly on the extended cold plate.

end temperature of the current lead as shown in Fig. 5. It is carried out numerically by solving Eq. (7) using finite difference and dividing length into small elements of length Δz. The evaluation of temperature development consists of program initialization, time loop with dynamically calculated time step Δt, and nested loop for temperature evaluation at each element of length Δz. The temperature at the two ends of the HTS lead depends on the temperature-dependent cooling power in the first and second stage of the cryo-cooler, respectively. The figure shows the propagation of normal zone due to sudden current overloading in given intervals of time. The result shows that rise of temperature is relatively slow initially but increases rapidly as the temperature increases. It is observed that by maintaining temperature at the warm end of the HTS current lead below 60 K facilitates safe operation from thermal runaway. Since the performance of the HTS leads depends on the magnetic field, the HTS current lead is placed in such a way that the radial magnetic field (B_r) should be minimum.

C. The HTS magnet

The HTS-based magnet coil is designed for the cryogen-free environment and mounted on a cold plate made of Oxygen-free High Conductivity Copper (OFHC) that has high thermal conductivity (in Fig. 6). This cold plate is in good thermal contact with the 2nd stage of CC2 by means of flexible links. It can carry maximum 60 kg of weight. The design ensures that the sample and magnet are thermally isolated.

The HTS-magnet coil under test is composed of 16 numbers of double pancake (DP) coils. Each DP coil is wound with relatively low tension on the bobbin by the wet winding method using Ag sheathed multi-filamentary Bi-2223 HTS tapes. The cooling of the magnet relies on high conductivity high purity copper disks inserted within the windings to extract heat efficiently into the mounting cold plate. All copper disks are divided by slots to smaller sections to reduce additional heat load generated by eddy current during charging and discharging operation. Design parameters of the magnet are shown in Table II.

The critical current of HTS conductors has a strong dependence against the radial component of the magnetic field, which has a maximum value at the magnet edges. In order to reduce this, radial field laminated iron sheets of 15 mm thickness are mounted at both the ends of magnet as shown in Fig. 7.

The axial field B_0 generated at the centre is about 2 T and given by[9]

$$B_0 = JAF(\alpha, \beta), \tag{11}$$

where $F(\alpha, \beta) = \mu_0 \beta \ln\left(\frac{\alpha+\sqrt{(\alpha^2+\beta^2)}}{1+\sqrt{1+\beta^2}}\right)$ and depends on the geometry of the coil. Here cross section of the coil is made to have a step consisting of co-axial coils with different lengths and is optimized to reduce the radial field with minimum amount of superconductor. The operating current margin is maintained within 70% of the critical current to avoid possible thermal runaway. The critical current depends on the maximum radial magnetic field for a given operating temperature of the magnet coil. It is obtained from the load line (I vs B_r), where B_r corresponds to the maximum radial field at the coil ends. The quenching of the magnet coil and normal zone propagation is simulated assuming coil as a whole homogenous and solving heat balance equation (7) numerically.[9] The quench is detected when the resistive voltage exceeds the threshold voltage for a given interval of time called validation time. A subsequently current decay follows the equation of a simple electric circuit consisting of external dump resistance R_d,

$$L_i \frac{dI}{dt} + [r(t) + R_d] I = 0. \tag{12}$$

Material properties of the individual winding constituents due to varying temperature and magnetic field are calculated. The estimated maximum hot spot temperature during quench

TABLE II. Design specifications of HTS magnet.

Coil type	Double pancake (DP)
No. of DP coils	16 no.
Moulding resin	Stycast/2850FT
Superconductor	HTS tape/DI-BSCCO (Sumitomo make)
HTS tape dimension	4.8 mm width/0.45 mm thick
Coil inner diameter	90 mm
Coil outer diameter	190 mm
Height of the coil	170 mm
Working bore	70 mm
Central field	>2 T
Maximum radial field in the coil region	<1 T
Operating current	160 A
Operating temperature	<30 K
Cold mass	~50 kg

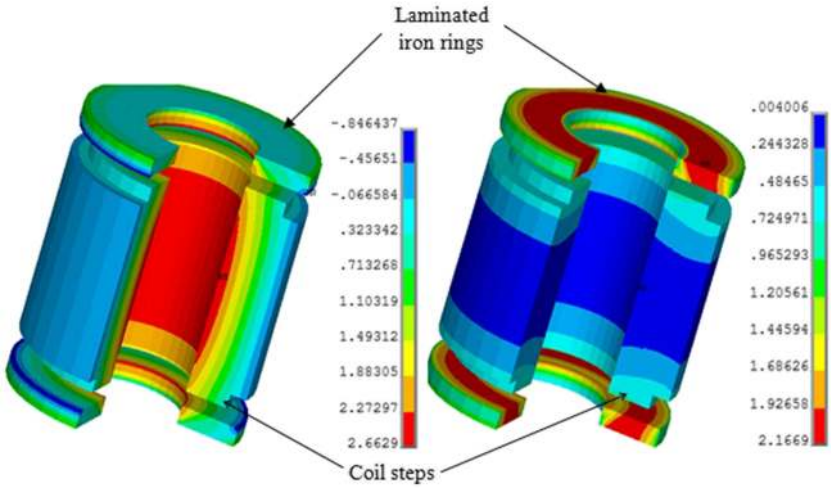

FIG. 7. Axial and radial field inside the magnet coil. The radial field is reduced using steps and laminated iron rings on both ends.

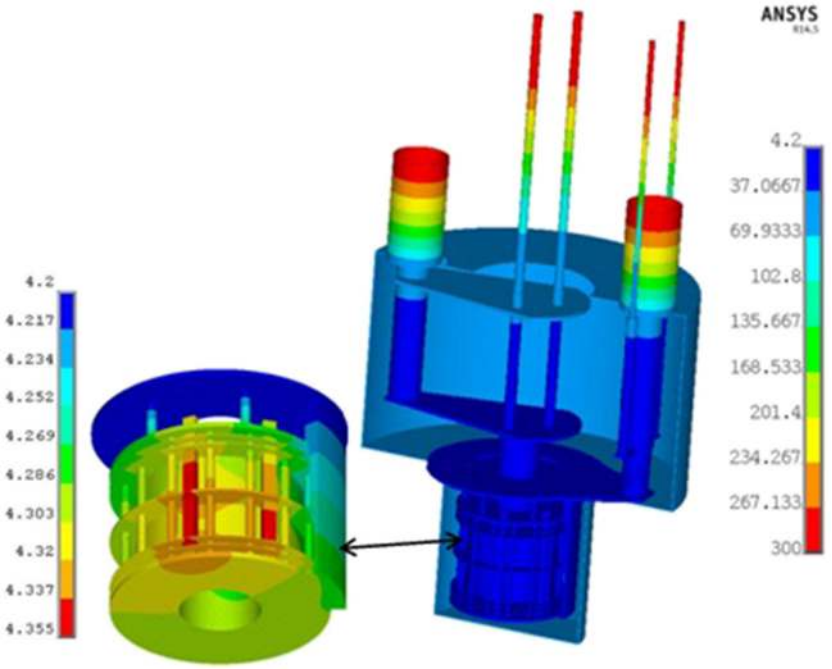

FIG. 8. Temperature distribution in the magnet coil under steady state condition. Temperature variation in the coil is less than 0.5 K.

is limited to 100 K using external dump which dissipates most of the stored energy. The stress level is calculated to be well within the limit that a HTS tape can withstand.

1. Integration of the magnet and cryo-cooler

The magnet was cooled down by using high purity copper braid as a flexible thermal link to connect the magnet with the 2nd stage of CC2. In order to avoid the decrease of cooling capacity caused by the influence of the magnetic field, the cold head is positioned to keep the leakage magnetic field of less than 0.3 T and below 500 G for the motor.[10] The flexible braided copper wire is used for compensation of thermal stress between the cold plate and the heat sink of the magnet during cool-down. The cross section of each connecting braid is optimised for a given length at different locations. Thin copper disks inserted at both ends of each of the coil are thermally connected to the cooling plate. To ensure uniform temperature distribution in the coil, the size of the copper plate and thermal path to the cryo-cooler are optimised. Thermal analysis is carried out using engineering simulation software ANSYS for coils and cooling structures. It is found that the maximum temperature difference between the cold head and the farthest

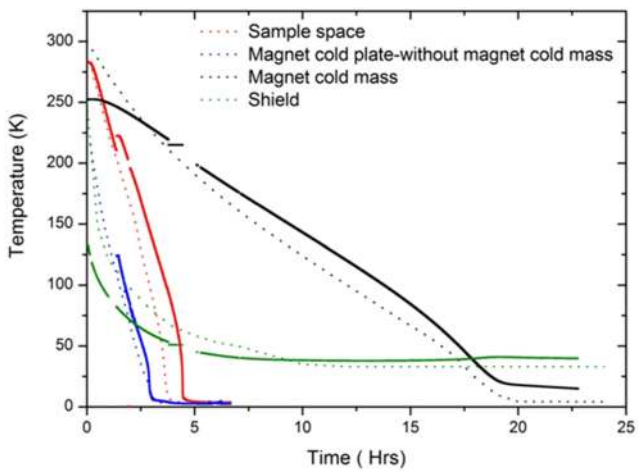

FIG. 9. Cool-down history under two situations (with and without magnet cold mass) along with simulated time.

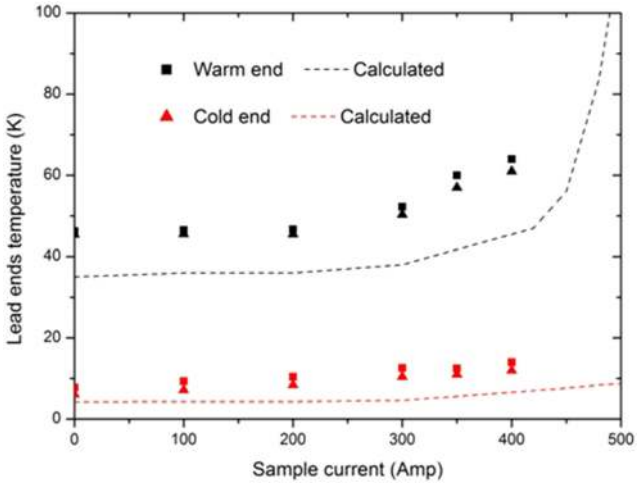

FIG. 10. Increase of temperature due to current at the warm end side of the HTS current lead. We maintained temperature below 60 K.

end of the coil is less than 1 K using a 1 mm thick copper plate (Fig. 8). The simulation is carried out assuming joint resistance of 1 $\mu\Omega$ for all the pancake coils connected in series and a magnet carrying 300 A of current. All the coils are stacked together and held tightly against the end plates with brass rods.

III. RESULTS OF PERFORMANCE TEST

The result of temperature measurement during cool-down at the sample space, radiation shield, of the magnet cold mass with/without magnet, and across current leads with current in the steady state is shown in Figs. 9 and 10, respectively.

It is noticed that the sample space reaches a temperature of 4.2 K from room temperature within about 5 h. As regards to the radiation shield, the temperature remains the same in both cases, with and without the magnet cold mass. The shield connected to the 1st stage of CC2 reaches final temperature of ~40 K in nearly 6 h for both cases. As the ruthenium temperature sensors attached to the radiation shield and magnet cold plate are calibrated for the temperature below 150 K, we could monitor temperature after about 150 K. A set of CERNOX temperature sensors are mounted at different locations around magnet coils to monitor its temperature during cool-down and energisation. Initially, without the magnet cold mass, it took about 5 h to cool down the cold plate from 300 K to 5 K as shown in Fig. 9. With magnet coil mounted, it took more than 20 h to reach the operating temperature using CC2. The heat penetration to the magnet cold mass is estimated to be about 5 W using the cooling load map and the value of its final temperature. It is observed that the temperature of the cold mass (sample space/superconducting magnet) decreases almost at a constant rate but drops sharply near 50 K. This may be attributed to marked rise in thermal conductivity of the copper lead toward the first stage, thereby reduces the spatial temperature gradient. It may be noted that experimental results are in agreement with the simulated output.

As the operating temperature and thermal stabilisation are attained, different performance tests are carried out successively by passing current in the sample and magnet circuit. Our measurement is restricted to current of 400 A for short samples as the temperature of the warm ends of the HTS lead increases rapidly as shown in Fig. 10. Voltage is measured using the voltage taps provided at the ends of the HTS leads, and it is found to increase continuously even when the temperature at the cold end of the HTS lead remains almost unchanged. Hence the high current operation was limited because of excessive Joule heating in the normal copper lead to the 1st stage of the CC1. The heat in-leak is about 20% more than the designed value at 400 A of current which is obtained by matching the measured temperature rise. As we have not considered the additional contact resistance (unknown) at the two ends of the HTS leads.

Available cooling power of the sample space and magnet circuit has been studied for this test setup as well (Fig. 11). We have carried out the thermal performance test by shorting

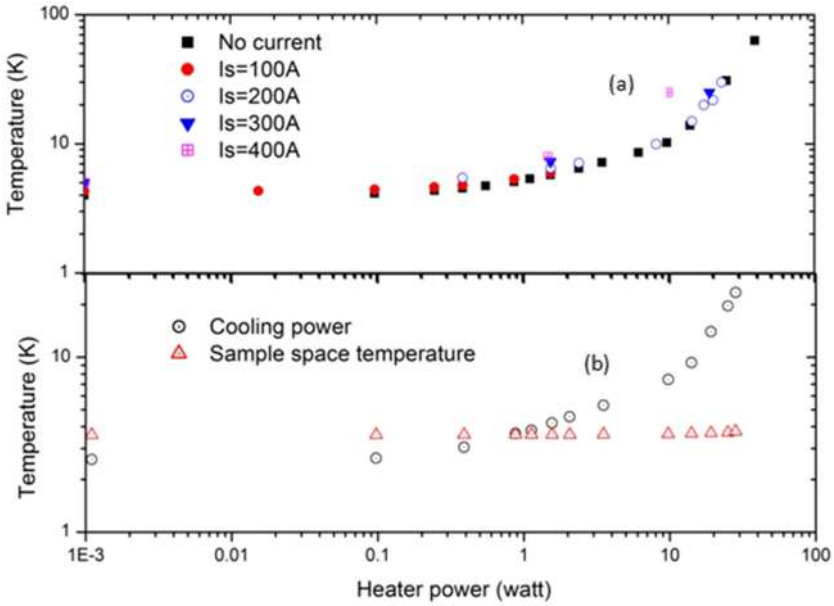

FIG. 11. (a) Available cooling power at a given temperature under different sample current, (b) measurement of cooling power with a heater attached to the magnet support plate. Also showing sample space temperature remains at 4 K during measurement indicating thermal isolation.

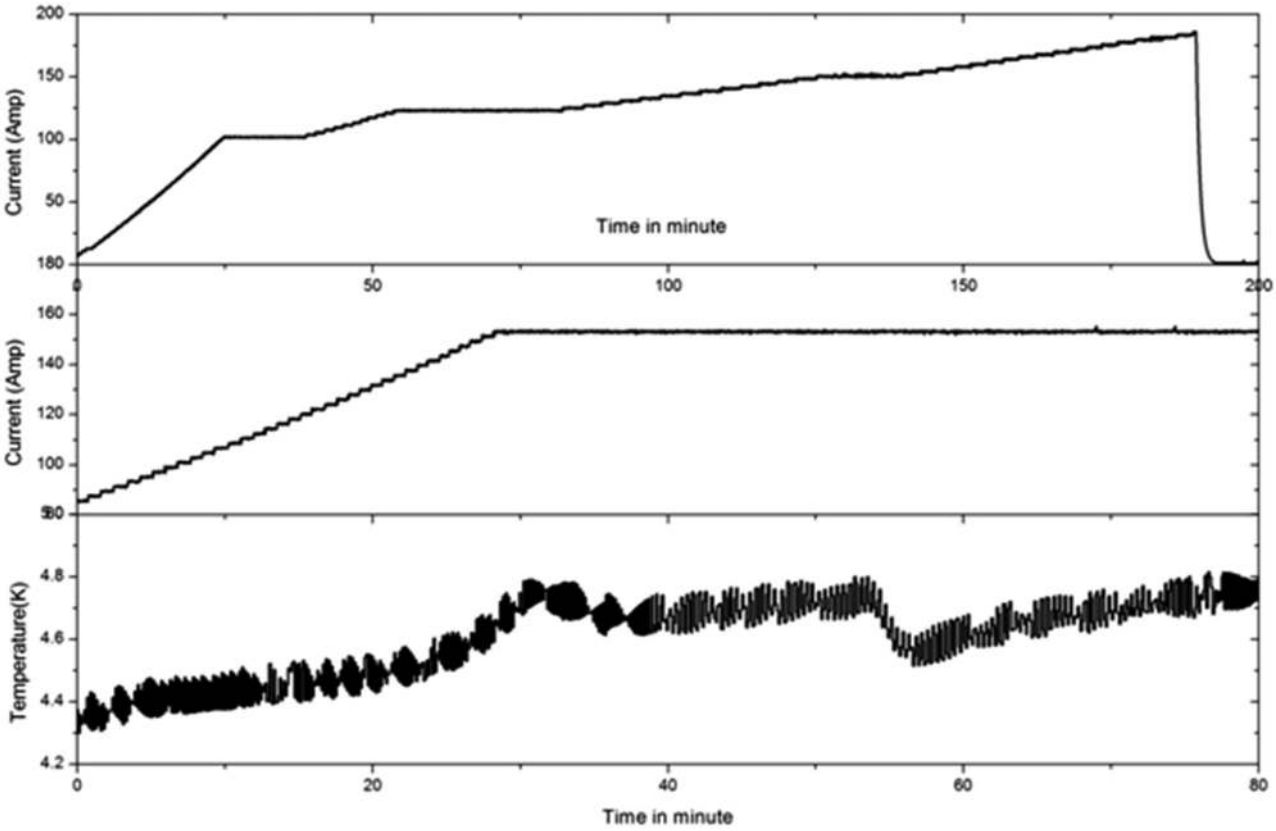

FIG. 12. Energisation of the magnet coil, which is made to quench at 186 A of current and continuous operation at design current of 160 A (B = 2 T) and corresponding magnet temperature.

with the HTS tape using a maximum of 400 A sample current. To give thermal load to the sample, a heater (40 W) is fixed on the plate anchored to the 2nd stage cold head of CC1. The current is passed through this heater and corresponding temperature is recorded under four different sample currents. The final temperature corresponding to a given sample current is plotted against heater power in the log scale and shown in Fig. 11(a). It is observed that about 40 W of heater power is needed to raise the temperature to about ~60 K without current.

As a way of characterising the HTS coil using the test setup, we have measured the temperature rise with thermal load at the second stage of CC2. In the present study, we shorted the magnet circuit with the HTS tape while passing a current

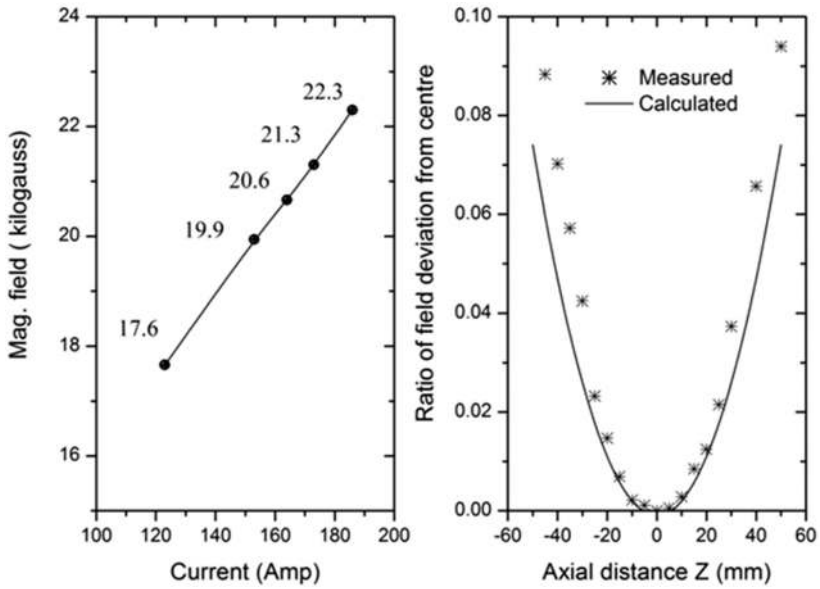

FIG. 13. Load line and field deviation along the z-axis of the magnet coil.

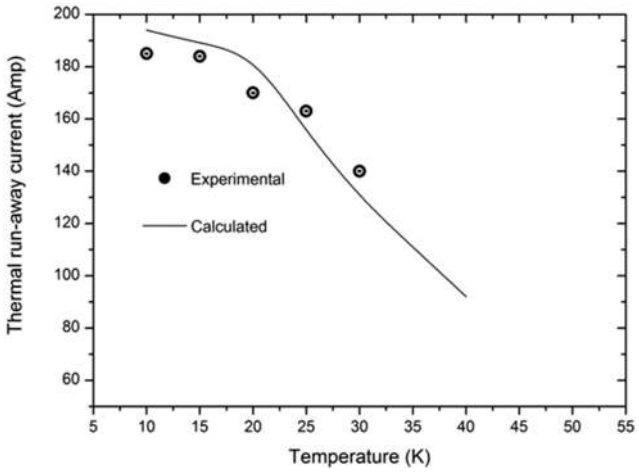

FIG. 14. Current at which the quench occurs at five different magnet temperatures.

of 300 A. The second stage of CC2 cools down the magnet circuit via a cold plate provided with a cartridge heater of 40 W. The temperature of the cold plate is plotted against the heater power as shown in Fig. 11(b). Evidently, the temperature can be maintained at 4.2 K with 1.3 W heater power on. As the specified cooling capacity of the second stage of CC2 is 1.5 W at 4.2 K, so the heat load is about 0.2 W at 4.2 K. If we continue increasing the heater power beyond 1.3 W, the temperature of the cold plate begins to rise. It is found that heater power of 25 W raises the temperature of the plate to 20 K, as seen from Fig. 12. During this measurement, the temperature at the warm ends of the HTS leads remains well within 60 K. Our experiment reveals that the magnet system is thermally isolated from the sample space because the temperature in the sample space remains constant at 4.2 K as displayed in Fig. 11(b).

Subsequently the HTS magnet coil is mounted on the cold plate cooled by CC2. As the superconducting coil reaches to equilibrium temperature, magnet current is ramped. To limit the ac losses during the first charging process, the current was initially ramped at 2 A/min up to 50 A, 1 A/min up to 120 A, and finally 0.5 A/min. It took about 2.5 h for the magnet to charge up to its operating current of 160 A and generate a magnetic field of 2 T, as shown in Fig. 12. Current is maintained for about 5 min at every current steps and magnetic field is measured. This ensures sufficient time for thermal stabilisation against dissipative ac losses during charging. We have operated the magnet continuously at the desired field of 2 T and monitor the temperature variation as shown in Fig. 12. The results show that the temperatures of the cold head and the magnet coils were stable during the entire process of measurement, indicating the good thermal behaviour of the coil structures. The measured fields are plotted against magnet currents in Fig. 13, which agrees with the calculations. To investigate field

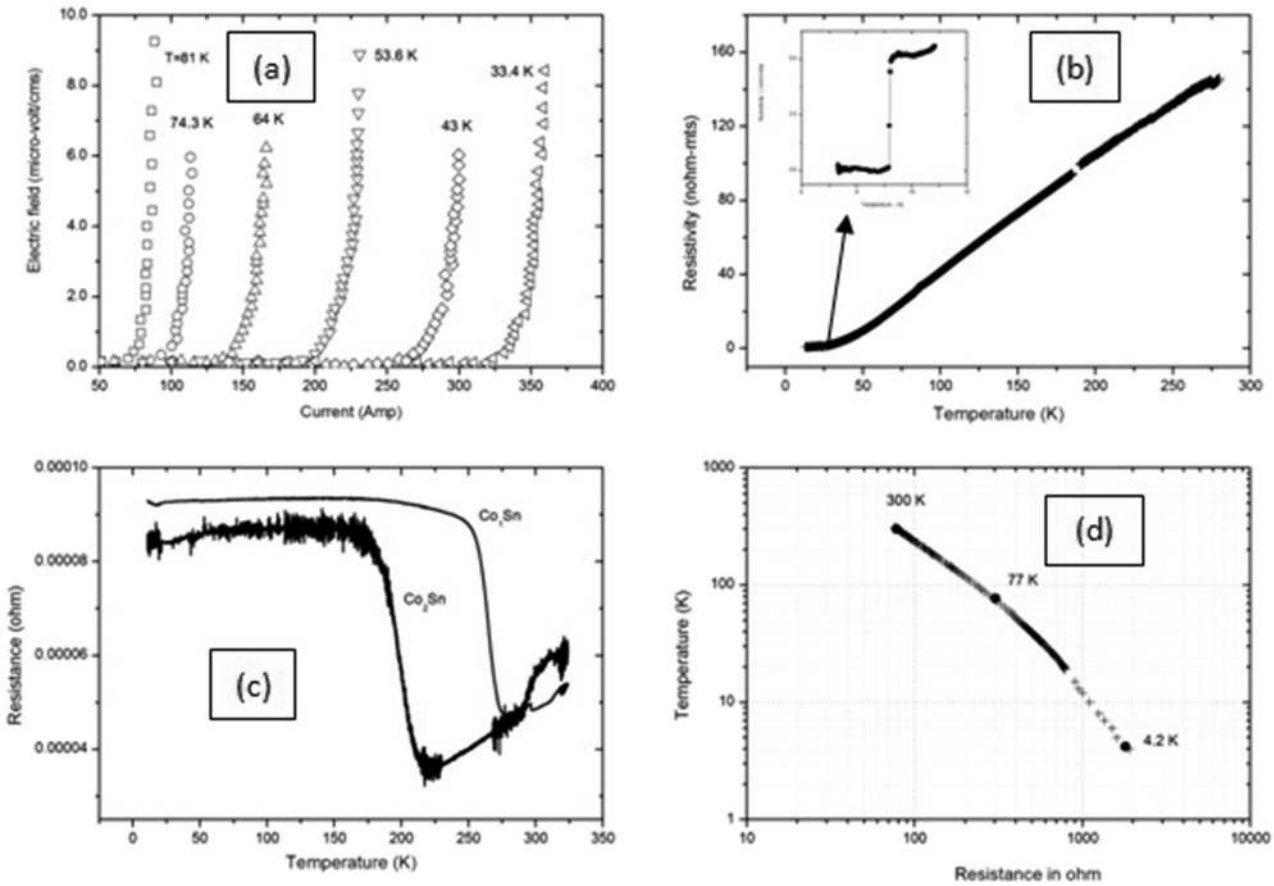

FIG. 15. Different measurements carried out using this test setup.

uniformity of the HTS magnet, magnetic field is measured in the z-direction with the magnet centre at z = 0. The results are plotted in terms of deviation from the centre field along with the calculated deviation in Fig. 13 and turns out to be within 10% at z = ±50 mm, which easily accommodate the sample vertical dimension.

We have verified the stability under different temperatures by measuring the thermal run-away currents as shown in Fig. 14. This is the maximum current that the coil can carry without undergoing thermal runaway for given temperature of the cold plate determined by the heater power. According to the measured results, the HTS magnet showed no performance degradation and the results agree well with the estimated value (Fig. 14).

This cryo-cooler based test setup is being used for different types of measurement as depicted in Fig. 15. We have carried out electrical characterisation of short HTS tape including joint resistance under different temperatures as shown in Fig. 15(a). The temperature of the sample varied using a sample heater, while passing a maximum current of 400 A. We have also measured residual resistivity ratio (RRR) of several niobium samples (9 mm diameter and 50 mm length) from different manufacturers [see Fig. 15(b)]. A study of phase transition phenomena in cobalt-tin samples with varying compositions is also done in this system at temperatures ranging from 4 K to 300 K [Fig. 15(c)]. Many temperature sensors are calibrated and compared with the values at three temperatures given by the supplier [see Fig. 15(d)]. The calibration is carried out against the standard diode sensor, which is glued side by side with four un-calibrated sensors in a common sample holder made of OFHC copper placed inside the iso-thermal copper chamber. We used quad-twisted cryogenic wires (Lake Shore) to get a four-terminal wiring of the sensor. The measurement was carried out during cool-down and warm-up (300 K ↔ 4.2 K) over a span of more than 24 h. The measurement uncertainty is less than ±0.1 K.

IV. CONCLUSIONS

A versatile cryogenic test setup has been built up in the laboratory at VECC. The system is successfully operated for large samples like the HTS magnet coil as well as small samples. The 2 T magnet has been designed and fabricated in-house and tested in this system. A 500 A current lead using the HTS tape is also made for the test setup. Results of performance tests reveal important characteristic features of the magnet coil as well as the HTS current lead. The thermal run-away current for the magnet coil at different temperatures and correlation between heater power and corresponding rise of temperatures at the sample and magnet circuit have been examined. The system envisages potential applications for low temperature measurement with high current and magnetic field up to 2 T.

ACKNOWLEDGMENTS

Authors are sincerely thankful to Shri Amitava Roy, Director, Variable Energy Cyclotron Centre, Kolkata, India for his generous support and encouragement during this work.

NOMENCLATURE

Subscripts

S	Thermal shield
M	Magnet
$A_{1,2}$	Thermal link—1st stage and 2nd stage
L	2nd stage temperature mass/low temperature side
H	1st stage temperature mass/warm temperature side
$c_{1,2}$	Load to cold head 1 and cold head 2
k	conduction
r	Thermal radiation
l	current lead
c	cold/lower part
1	Room temperature to 1st stage, i.e., thermal shield
2	1st stage to 2nd stage, i.e., magnet/cold mass

Symbol

HTS	High Temperature Superconductor
I_c	Critical current
CC1 and CC2	Cryo-cooler 1 and cryo-cooler 2
RRR	Residual Resistivity Ratio
C	Heat Capacity
T	Temperature
t	Time
Q	Heat flow
TAK	Thermal Analysis Kit
I	Current
z	Length/Axial distance
A	Cross section
k	Thermal conductivity
ρ	Electrical resistivity
L	Current lead length
OFHC	Oxygen Free High Conductivity
DP	Double pancake
J	Current density
B_0	Magnetic field at centre
B_r	Radial magnetic field
μ_0	Magnetic permeability
α	Ratio of outer radius to inner radius of coil
β	Ratio of length to inner radius of coil
L_i	Inductance of coil
r(t)	Coil resistance with time t
R_d	External dump resistance

[1]H. J. M. ter Brake and G. F. M. Wiegernick, Cryogenics **42**, 705–718 (2002).
[2]G. Snitchler *et al.*, IEEE Trans. Appl. Supercond. **9**, 553–558 (1999).
[3]L. Kopera, P. Kovac, and T. Melisek, IEEE Trans. Appl. Supercond. **16**, 1415–1418 (2006).
[4]M. H. Sohn *et al.*, Phys. C **471**, 1449–1453 (2011).
[5]J. Pradhan *et al.*, paper presented at the 7th Asian Conference on Applied Superconductivity and Cryogenics, Conference, Turkey, 2013.
[6]Y. Suk Choi *et al.*, Cryogenics **52**, 13–18 (2012).
[7]H. M. Chang *et al.*, Cryogenics **42**, 787–794 (2002).
[8]Thermal Analysis Kit and K & K Associates, Westminster, Colorado, USA.
[9]M. N. Wilson, *Superconducting Magnets* (Oxford University Press, 1983).
[10]W. Ma *et al.*, IEEE Trans. Appl. Supercond. **22**(5), 4905605 (2012).